Ultrafast demagnetization in Ni: theory of magneto-optics for non-equilibrium electron distributions

2004 J. Phys.: Condens. Matter 16 5519

(http://iopscience.iop.org/0953-8984/16/30/013)

INSTITUTE OF PHYSICS PUBLISHING JOURNAL OF PHYSICS: CONDENSED MATTER

J. Phys.: Condens. Matter **16** (2004) 5519–5530 PII: S0953-8984(04)81203-7

Ultrafast demagnetization in Ni: theory of magneto-optics for non-equilibrium electron distributions

P M Oppeneer[1,2] **and A Liebsch**[3]

[1] Leibniz-Institute of Solid State and Materials Research, PO Box 27006, D-01171 Dresden, Germany
[2] Department of Physics, Uppsala University, Box 530, S-751 21 Uppsala, Sweden
[3] Institut für Festkörperforschung, Forschungszentrum Jülich, D-52425 Jülich, Germany

Received 25 May 2004
Published 16 July 2004
Online at stacks.iop.org/JPhysCM/16/5519
doi:10.1088/0953-8984/16/30/013

Abstract

The sensitivity of the magneto-optical Kerr response to electronic thermalization processes in ultrafast pump–probe experiments is studied by evaluating the complex conductivity tensor of Ni for non-equilibrium electron distributions. The electronic structure and optical matrix elements are calculated within density functional theory. To account for the electronic redistributions generated by the intense pump-laser pulse during the initial stages of electronic thermalization, two kinds of model electron distributions are considered which mimic the so-called dichroic bleaching or state-blocking effect. Thus, certain optical transitions which are allowed under equilibrium conditions are not accessible to the probe laser. It is shown that the conductivity tensor and the complex Kerr angle can be modified substantially by the non-equilibrium electron distributions. Moreover, in striking contrast to the case for ordinary equilibrium conditions, the Kerr rotation and ellipticity are no longer proportional to the magnetization of the sample. The Kerr response at ultrashort times can therefore not be taken as a measure of demagnetization.

(Some figures in this article are in colour only in the electronic version)

1. Introduction

The magnetization dynamics of itinerant ferromagnets down to femtosecond timescales plays a key role in modern technologies such as magnetic recording and spin electronics. Several experimental techniques have been used to investigate the magnetization dynamics: pump–probe magneto-optical Kerr effect (MOKE) measurements [1–3], time-dependent two-photon photoemission investigations [4, 5], and second-harmonic generation studies [6–9]. In these experiments, intense ultrashort laser pulses generate electron distributions far from

equilibrium and thereby give rise to demagnetization processes. The details of how the system's magnetization is changed—in particular, the role of spin–orbit interaction—are so far not well understood. While electron–electron interactions dominate the initial time interval of about 100 fs during which the electron gas thermalizes, the electron–phonon interaction is responsible for the subsequent energy transfer to the lattice (see, e.g., [10]).

An important but controversial issue concerns the spin dynamics in the sub-picosecond time regime right after the pump-laser pulse is switched off. Pump–probe magneto-optical Kerr experiments carried out on Ni and $CoPt_3$ films showed a sharp drop in the Kerr signal that was interpreted as a demagnetization occurring within a few hundred fs [1, 11]. This interpretation was supported by theoretical considerations for Ni claiming ultrafast demagnetization within 20 fs [12, 13]. Other studies, however, suggested a fundamentally different scenario [3, 9, 14]. In particular, time-resolved measurements of the Kerr effect for Ni by Koopmans *et al* [3, 15] showed that in the sub-picosecond regime the Kerr rotation and ellipticity are not proportional to the magnetization, in contrast to the case for equilibrium conditions. Only after the electron gas has thermalized does the magneto-optical signal follow the temperature variation of the magnetization. To explain the observed discrepancy at short times Koopmans *et al* proposed a so-called dichroic bleaching or state-blocking mechanism. As a consequence of the intense pump laser certain optical transitions are saturated and not available to the subsequent probe laser. Investigations of the second-harmonic signal of a Ni film also indicated that the fast initial drop of the signal cannot be unambiguously attributed to ultrafast demagnetization [9]. Time-resolved MOKE studies on $CoPt_3$ [16] and Fe films [14] observed considerable nonmagnetic contributions caused by the non-equilibrium distribution that persisted up to several picoseconds [16] or even longer [14, 17]. On the other hand, a recent time-resolved MOKE study on Ni films, carried out under somewhat different conditions, found no particular difference in the time dependence of the Kerr rotation and ellipticity [18].

In view of the fundamental and technological importance of ultrafast spin dynamics, more experimental and theoretical research is clearly needed to clarify the role of the non-equilibrium electron distributions in probing the magnetic response. The aim of the present work is to investigate the bleaching mechanism for Ni by performing detailed calculations of the optical conductivity tensor and complex Kerr angle for non-equilibrium electron distributions. Thus, we do not study the actual time dependence of the electronic density during the initial laser excitation and the subsequent thermalization via electron–electron collisions. This time dependence is exceedingly complex and would require the solution of the many-body Schrödinger equation in the presence of an intense laser field. Instead, we consider 'snapshots' of plausible non-equilibrium distributions generated by the pump laser and ask to what extent these distributions reveal information on the magnetization of the sample if they are detected via a probe laser. Thus, we are primarily concerned with the 'hypothetical' time window right after the pump laser is switched off and before electronic thermalization sets in.

The non-equilibrium distributions are represented via step-like functions of the energy based on the following two complementary models. For a given pump-laser frequency ω_p and fluence F, model A treats the relative occupations within $E_F \pm \hbar\omega_p$ near the Fermi energy E_F mainly according to the density of states (DOS) of the various spin bands involved. The laser fluence determines the total number n_p of electrons excited per Ni atom. A similar approach had been used in the description of non-equilibrium electron distributions for Au solids and particles [19, 20]. Model B focuses on the fact that the pump laser blocks pairs of spin bands separated by $\hbar\omega_p$. Thus, instead of specifying occupations of individual spin bands, this model considers differences between band occupations, just as they appear in the expression for the conductivity tensor. While these models can only provide qualitative estimates of the role of non-equilibrium electron distributions in magneto-optical spectroscopies, they clearly

indicate that the state-blocking mechanism must be taken into account in the interpretation of the MOKE signal. In particular, they suggest that the complex Kerr angle at ultrashort times is not proportional to the sample magnetization.

The outline of this paper is as follows. In section 2 we discuss the evaluation of the complex conductivity tensor within density functional theory and specify the modification of the band occupations appropriate for non-equilibrium electron distributions. The results are discussed in section 3 and our conclusions are given in section 4.

2. Theory

2.1. Ab initio calculation of the MOKE

Linearly polarized light reflected from the surface of a magnetic material provides information on the magnetism of the sample. In the so-called polar geometry, where both the incident wavevector and the magnetization are perpendicular to the surface, the polarization vector of the reflected light beam is rotated with respect to that of the incident beam and the reflected light is elliptically polarized. The complex polar Kerr angle Φ_{K} can be written in terms of the macroscopic conductivity tensor $\sigma_{ij}(\omega)$. If the z axis is chosen normal to the surface, the Kerr angle is given by

$$\Phi_{\mathrm{K}} \equiv \theta_{\mathrm{K}} + \mathrm{i}\varepsilon_{\mathrm{K}} = \frac{-\sigma_{xy}}{\sigma_{xx}(1 + \mathrm{i}\frac{4\pi}{\omega}\sigma_{xx})^{1/2}}, \tag{1}$$

where θ_{K} is the real Kerr rotation angle and ε_{K} the Kerr ellipticity. In the single-particle picture the interband contributions to the components $\sigma_{ij}(\omega)$ may be obtained from the standard linear-response formula ($i,\ j = x,\ y$):

$$\sigma_{ij}(\omega) = \frac{\mathrm{i}e^2}{m^2\hbar V}\sum_{\boldsymbol{k}}\sum_{\alpha<\alpha'}\frac{f_\alpha(\boldsymbol{k}) - f_{\alpha'}(\boldsymbol{k})}{\omega_{\alpha'\alpha}(\boldsymbol{k})}\left(\frac{\Pi^i_{\alpha\alpha'}(\boldsymbol{k})\Pi^j_{\alpha'\alpha}(\boldsymbol{k})}{\omega - \omega_{\alpha'\alpha}(\boldsymbol{k}) + \mathrm{i}\delta} + \frac{(\Pi^i_{\alpha\alpha'}(\boldsymbol{k})\Pi^j_{\alpha'\alpha}(\boldsymbol{k}))^*}{\omega + \omega_{\alpha'\alpha}(\boldsymbol{k}) + \mathrm{i}\delta}\right), \tag{2}$$

where α denotes a relativistic band index, i.e., a combined band n and spin σ index. The Fermi distribution is denoted by $f_\alpha(\boldsymbol{k})$, $\hbar\omega_{\alpha'\alpha}(\boldsymbol{k}) = E_{\alpha'}(\boldsymbol{k}) - E_\alpha(\boldsymbol{k})$ is the energy difference between an unoccupied band α' and an occupied band α, and $\delta = 1/\tau$ specifies a phenomenological relaxation time of the excited state (see, e.g., [21]). The $\Pi_{\alpha\alpha'}$ are matrix elements of the momentum operator which we approximate as $\boldsymbol{p} = -\mathrm{i}\hbar\boldsymbol{\nabla}$. This choice for $\boldsymbol{p}$ excludes spin-flip optical transitions which can be present when a relativistic form for $\boldsymbol{p}$ based on the Dirac equation is adopted. However, it has been shown that such spin-flip contributions are negligible [22]. As a consequence, the optical transition matrix elements are spin diagonal.

In addition to the interband contribution to the conductivity, there is the intraband conductivity arising from electron scattering via impurities and phonons. This term is important primarily at low excitation energies and can be described in terms of an empirical Drude function, i.e., $\sigma_{\mathrm{D}}(\omega) = \sigma_0/(1 - \mathrm{i}\omega\tau_{\mathrm{D}})$, where the constants σ_0 and τ_{D} are usually taken from experiments. In the pump–probe experiments considered here, the laser photon energy is 1.7 eV [3]. The weak Drude tail at this energy can be ignored for θ_{K}. For ε_{K} the influence of the Drude term is more extended; however, this term is not expected to affect the pump–probe changes in the MOKE relative to the unperturbed signal.

The electronic properties are derived from spin-density functional theory in the local spin-density approximation (LSDA). Band energies and wavefunctions are evaluated using the augmented spherical wave (ASW) method [23]. As discussed in [21] both real and imaginary parts of the conductivity elements are obtained via an analytical tetrahedron Brillouin-zone (BZ) integration technique, thereby avoiding a Kramers–Kronig integration. In the case of

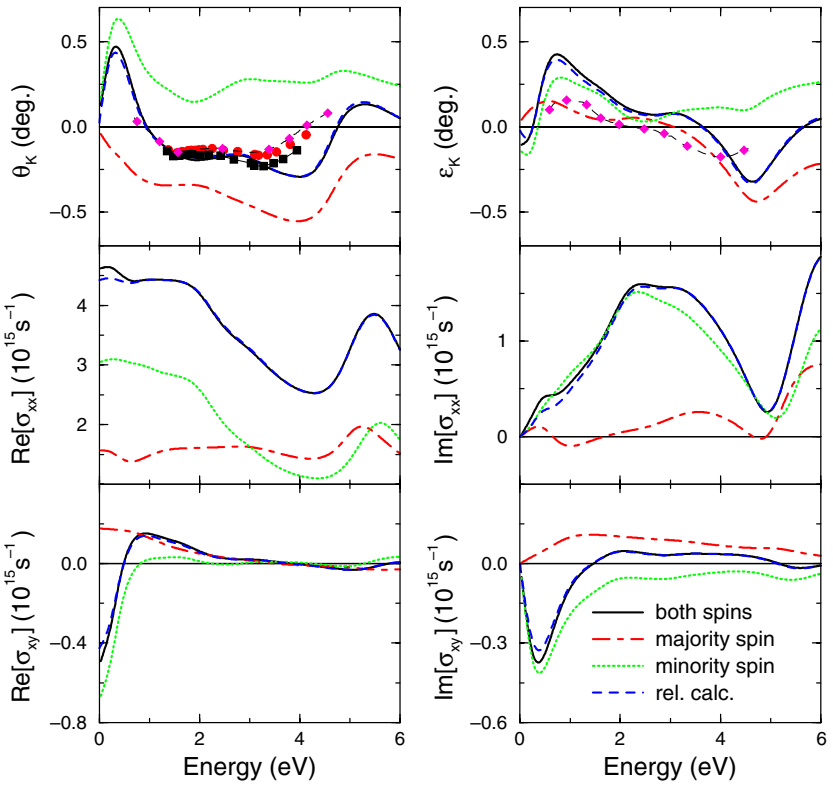

Figure 1. Total and spin-projected contributions to the interband optical conductivity tensor $\sigma_{ij}(\omega)$ and complex polar Kerr angle of Ni. Black solid curves: both spins; dashed–dotted curves: the majority-spin channel; dotted curves: the minority-spin channel; dashed curves: results of a relativistic calculation (see the text). The top panels also show the experimental Kerr rotation and ellipticity of van Engen [25] (— ♦—) for 300 K and those of Di and Uchiyama [26] for 300 K (●) and 85 K (—■—).

Fe, the results for $\sigma_{ij}(\omega)$ agree very well with available experimental results and the magneto-optical polar Kerr rotation is predicted to within a few per cent [21, 24]. As shown in figure 1, the calculations for Ni reproduce the measured Kerr rotation [25, 26] rather well at laser energies below 3 eV. The lifetime broadening is $\hbar/\tau = 0.4$ eV ($\tau \approx 1.6$ fs). The calculated Kerr ellipticity follows the shape of the measured ellipticity [25], but is larger and shifted because the Drude contribution is neglected. In the range 3.5–5 eV a discrepancy arises for both θ_K and ε_K which is associated with the well-known approximate nature of the LSDA for the description of moderately correlated materials. In Ni electronic correlations beyond the LSDA lead to a reduced exchange splitting between majority- and minority-spin bands as well as a narrowing of the 3d band [24]. In addition, in photoemission experiments (but not in optical experiments) strong quasi-particle damping and a satellite at 6 eV binding energy occur [27].

The microscopic mechanism underlying MOKE is spin–orbit coupling [28, 29]. Since it is quite small for 3d transition metals we include it within a second variational treatment. The resulting Bloch functions are sums of spin-up and spin-down scalar-relativistic functions that can be projected onto spin-diagonal functions. The band energies are nearly spin diagonal. At crossings of scalar-relativistic bands with opposite spin character the spin degeneracy is

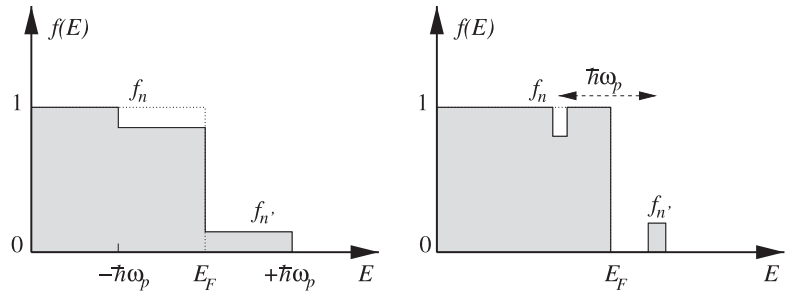

Figure 2. Models of non-equilibrium electron distributions generated by a pump laser of energy $\hbar\omega_{\mathrm{p}}$ (schematic). Left panel: model A. The deviation from unity below E_{F} and from zero above E_{F} give the depletion of state n and state filling of state n', respectively, caused by the laser fluence. Right panel: model B. The pump laser causes a depletion of a state n and a filling of state n' separated by an energy $\hbar\omega_{\mathrm{p}}$.

lifted by the spin–orbit coupling. To consider the influence of state-blocking effects in the separate spin channels we approximate $f_\alpha(\boldsymbol{k})$ by one spin type in k-space regions of the size of an integration tetrahedron. Thus, in these regions the effect of spin mixing on the occupation number is ignored. This is a reasonable approximation since spin–orbit coupling is weak and the band energies are almost spin diagonal.

Figure 1 also shows the calculated total and spin-projected components of the interband conductivity tensor and complex Kerr angle. The results are shown for a spin-diagonal and spin-non-diagonal treatment of f_α. The close resemblance of these spectra proves that the spin-diagonal assumption is adequate. Furthermore, the spin decomposition indicates that the spin channels have roughly opposite effects on the Kerr angle (it vanishes in the paramagnetic case). Thus, the spontaneous Hall conductivity—$\mathrm{Re}[\sigma_{xy}(0)]$—is predicted to have opposite signs for the two spin channels.

Although expressions (1), (2) are strictly valid only under equilibrium conditions we use them in the following sections to qualitatively describe the sensitivity of the conductivity tensor to small deviations from this limit. The demagnetization experiment for Ni [3] which we address involved very small laser induced modifications of electronic occupation numbers, corresponding to roughly 0.3% of the electrons within the 1.7 eV window reached by the laser. This deviation from equilibrium is sufficiently small for expressions (1), (2) to remain qualitatively applicable. The considerable advantage of these expressions is that they provide a detailed picture of all the important optical transitions contributing to the complex MOKE signal. In particular, we emphasize that density functional theory gives an excellent representation of these transitions and that, as a result of vertex cancellations, Coulomb correlations are negligible. In the following we focus on the spectral region near the laser frequency 1.7 eV and investigate the effect of dichroic bleaching on the components of $\sigma_{ij}(\omega)$ and on the complex Kerr angle.

2.2. Model A: non-equilibrium distributions for occupied and unoccupied states

Our aim is to derive band and spin-dependent occupation numbers which serve as input for calculating the non-equilibrium magneto-optical Kerr response. In the simplest form, a non-equilibrium electron distribution can be generated by the pump laser with energy 1.7 eV as follows. As schematically indicated in figure 2, occupied bands down to 1.7 eV below E_{F} can be partially depleted and previously unoccupied bands up to 1.7 eV above E_{F} can be partially

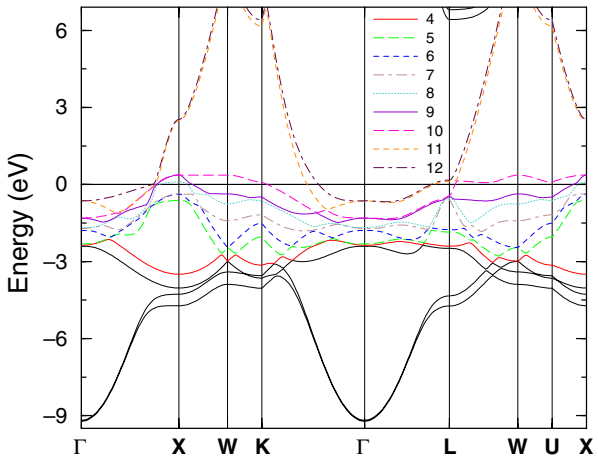

Figure 3. The relativistic energy bands of fcc Ni, calculated within the LSDA. The numbers denote band indices (counted from the bottom of the valence band).

populated. Thus, instead of the $T = 0$ Fermi distribution we have spin-dependent step-like non-equilibrium distributions [10, 19, 20].

To compute the occupation numbers f_α in the windows $E_F \pm 1.7$ eV we take advantage of several input data. According to the spin decomposition of the absorptive spectrum $\mathrm{Re}[\sigma_{xx}]$ shown in figure 1 about 63% of the transitions at 1.7 eV occur in the spin-down channel. To illustrate the more detailed band decomposition of $\mathrm{Re}[\sigma_{xx}]$ we show in figure 3 the band structure of fcc Ni. Only three unoccupied bands are relevant: bands 10, 11, and 12, the first of which is the empty part of the d band while the latter two are dispersive sp bands. The occupied bands (5–10) are essentially all d-like. To determine which fractions of electrons are excited into the three unoccupied bands we consider the band and spin decomposition of the elements of the optical conductivity tensor, as shown in figures 4 and 5 for majority- and minority-spin transitions, respectively (calculated for $\hbar/\tau = 0.1$ eV). Figure 4 reveals that close to 100% of the majority-spin transitions at 1.7 eV go into band 11. On the other hand, from the results shown in figure 5 for $\mathrm{Re}[\sigma_{xx}]$ we find that 63% of the spin-down transitions go into band 10, 4% into band 11, and 33% into band 12. Figures 4 and 5 furthermore indicate that state blocking can affect $\mathrm{Re}[\sigma_{xx}]$ in a manner different from $\mathrm{Re}[\sigma_{xy}]$ and $\mathrm{Im}[\sigma_{xy}]$. For $\mathrm{Re}[\sigma_{xx}]$, state blocking will always reduce the spectral intensity, whereas for σ_{xy}, the influences of state blocking in different band combinations may compensate one another. Also, some band combinations exhibit a strong optical response, but a small magneto-optical response and vice versa (see, e.g., the transition of band 4 to band 10 in figure 5). To determine the occupation numbers we make use, in addition, of the number of electrons each of the bands 10, 11, and 12 can accommodate in the 1.7 eV energy window. Integrating the density of states we find that the available unoccupied bands can accommodate 0.25 majority-spin and 0.74 minority-spin electrons. Specifically, band 11 contains 0.245 spin-up electrons while bands 9, 10, 11, and 12 comprise 0.01, 0.38, 0.02, and 0.33 spin-down electrons, respectively.

From these input data the various occupation numbers for the non-equilibrium distribution can now be estimated. Let us assume that n_p electrons per Ni atom are excited by the pump laser. Of these n_p electrons, $0.366\,n_p$ are spin-up and $0.634\,n_p$ are spin-down electrons. Thus, the spin-up occupation number for the unoccupied band 11, which receives 98% of the majority-spin electrons, becomes $f^{>}_{11,\uparrow} = 0.98 \times 0.366\,n_p/0.245$. The occupation numbers of the other unoccupied bands can be calculated analogously. In the energy window 1.7 eV below E_F we adopt a somewhat simpler approach since there are several flat bands with similar transition strengths. We therefore distinguish only spin-dependent occupation

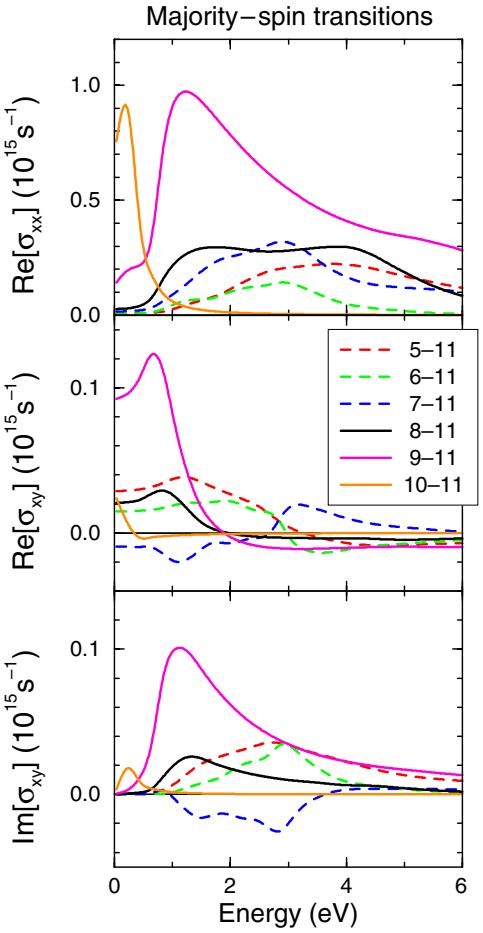

Figure 4. Band-by-band decomposition of the Re$[\sigma_{xx}]$, Re$[\sigma_{xy}]$, and Im$[\sigma_{xy}]$ optical conductivity spectra of Ni for the majority-spin channel. Only the dominating optical transitions are shown.

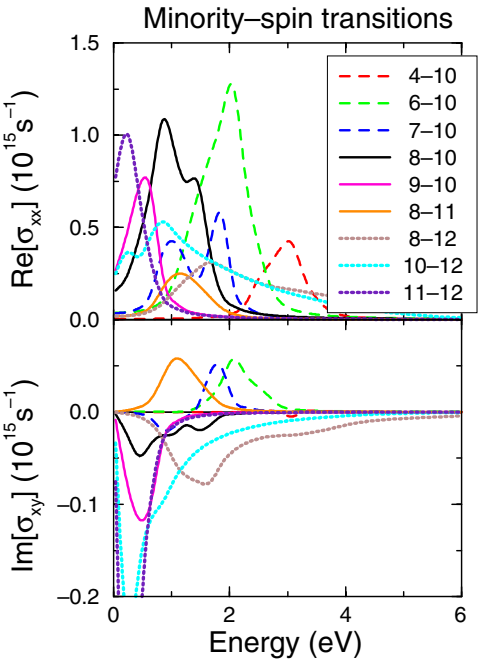

Figure 5. As figure 4, but for the minority-spin channel and only for the absorptive spectra Re$[\sigma_{xx}]$ and Im$[\sigma_{xy}]$.

numbers. Integrating the density of states we obtain 1.81 majority-spin and 1.77 minority-spin electrons, respectively. Thus, the occupation numbers are $f^{<}_{n,\uparrow} = (1.81 - 0.366\,n_{\rm p})/1.81$ and $f^{<}_{n,\downarrow} = (1.77 - 0.634\,n_{\rm p})/1.77$.

The number of excited electrons per Ni atom was estimated by Koopmans *et al* [3] from the laser fluence to be $n_{\rm p} \approx 0.012$. This is a remarkably small value, which amounts to about 0.3% of the Ni valence electrons in the window 1.7 eV below $E_{\rm F}$ and about 1% of the empty states within 1.7 eV above $E_{\rm F}$. Inserting these values into the expressions for the non-equilibrium occupation numbers discussed above it is evident that the changes in the complex conductivity and Kerr angle are also of the order of 1%. As will be discussed further below, the reason for these small changes is the fact that in model A the electron and hole states created in the optical transition are spread independently of one another over a total energy region of $2\hbar\omega_{\rm p}$. As a result, the state-blocking mechanism is not very pronounced within this model. Nevertheless, in order to qualitatively illustrate the bleaching effect for model A we shall discuss results of calculations for laser fluences corresponding to $n_{\rm p} = 0.05$ and 0.10.

2.3. Model B: non-equilibrium distributions for pairs of occupied and unoccupied states

The step-like non-equilibrium distribution of model A is plausible and has been considered recently for several systems [10, 19, 20]. As pointed out above, however, it is clear that the specific state blocking occurring in optical measurements (as opposed to electron injection or emission experiments, for instance) is not incorporated in this model. Rather than considering the individual occupations of states below and above E_F, optical transitions require treatment of pairs of states separated by the laser frequency. As already noted by Koopmans *et al*, due to the Ni band structure the important excitations take place from rather flat filled bands to dispersive empty bands, causing a substantial filling of the dispersive band in a small energy interval near the initial band energy plus the energy of the pump laser [30]. Instead of spreading the excited electrons and holes uniformly over the energy windows $E_F \pm \hbar\omega_p$, we now explore in model B the opposite limit where only transitions between those pairs of occupied and empty states whose energies differ by $\hbar\omega_p$ are partially blocked. Consider, for example, the important transition from band 9 to band 11 in the majority-spin channel (see figure 2). In view of the flat dispersion of band 9 and the small k-space region in which the direct transition to band 11 occurs, state blocking should indeed take place in a very small energy interval—an interval very much smaller than the 1.7 eV window assumed in model A.

To estimate the occupation numbers within model B we proceed as follows. First we determine the number of electrons that can be excited in a spectral interval localized close to the laser frequency. A convenient way to compute this number is to use the optical sum rule $\int \mathrm{Re}[\sigma_{xx}(\omega)]\,\mathrm{d}\omega = C\,N_{el}$ (see, e.g., [24]). Here C is a constant and N_{el} is the number of valence electrons. For example, according to the calculated optical conductivity the energy interval from 1.6 to 1.8 eV corresponds to excitation of 0.037 electrons. More generally, we denote by n_{tot} the maximum number of electrons absorbed within an energy interval of width D about $\hbar\omega_p = 1.7$ eV. It is now straightforward to estimate the difference $f^<_{n\sigma} - f^>_{m\sigma}$ for pairs of bands, which is the quantity required for the evaluation of the conductivity tensor (see equation (2)). From the band decomposition of $\mathrm{Re}[\sigma_{xx}(\omega)]$ (see figures 4 and 5) we know the fraction each transition contributes to the total intensity at 1.7 eV in a given spin channel. Denoting this by $r_{nm\sigma}$ we find $f^<_{n\sigma} - f^>_{m\sigma} = 1 - (r_{nm\sigma}n_p/r_{nm\sigma}n_{tot}) = 1 - (n_p/n_{tot})$. The factor $r_{nm\sigma}$ drops out since it determines the fraction $r_{nm\sigma}n_p$ of electrons excited in the $nm\sigma$ channel as well as the fraction $r_{nm\sigma}n_{tot}$ of electrons that can maximally be excited within this channel.

Model B has the advantage that it explicitly considers the pairs of spin bands that are involved in the excitation process. The spectral region that is affected by the pump laser is confined to a window of width D in the immediate vicinity of the laser frequency. The width D is proportional to the intrinsic linewidth of the optical transition. The intrinsic linewidth in the frequency range considered is not known, but it is certainly smaller than the broadening of 0.4 eV adopted in the calculation of σ_{ij}, which accounts for the experimental resolution as well. We adopt here a narrow energy window $D = 0.2$ eV, on top of which the broadening 0.4 eV is applied. The narrowness of this window qualitatively confines the bleaching to those bands which directly contribute to the spectral intensity. Due to the flat dispersion of the d bands this also confines the bleaching to relatively small regions in k-space where the direct optical transitions to dispersive sp bands occur. As noted above, for $D = 0.2$ eV state depletion and filling involves about 0.037 electrons. Thus, for $n_p \approx 0.01$ as estimated by Koopmans *et al* [3] we find $f^<_{n\sigma} - f^>_{m\sigma} \approx 0.73$. Larger values of D lead to accordingly smaller deviations of $f^<_{n\sigma} - f^>_{m\sigma}$ from unity. Thus, the state-blocking mechanism in model B gives rise to changes of occupation numbers of the order of 10–20%. As shown below, modifications of similar magnitude are obtained for the optical conductivity and complex Kerr angle.

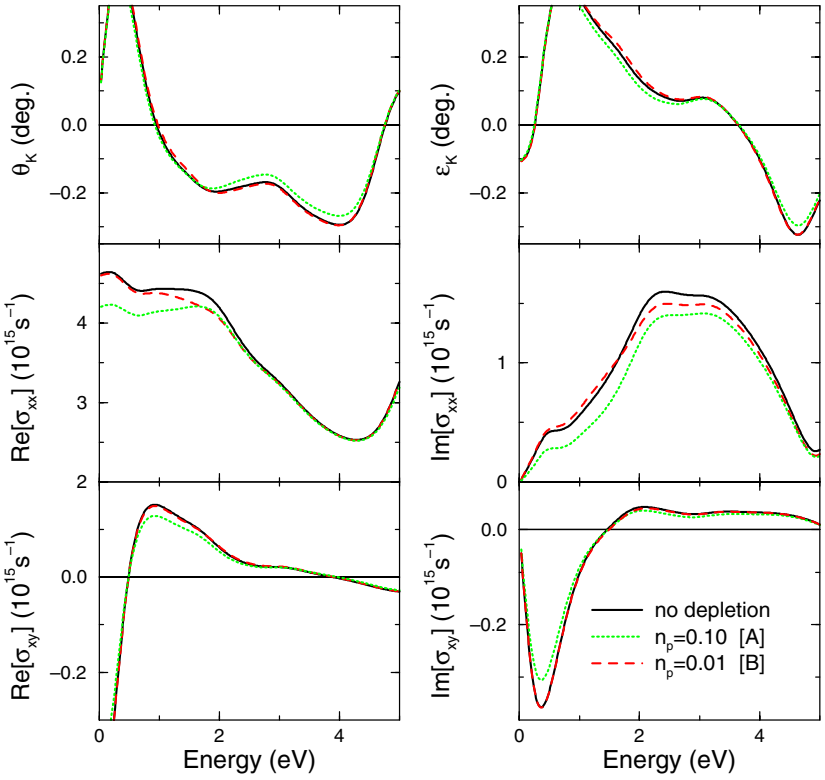

Figure 6. Calculated components of the conductivity tensor $\sigma_{ij}(\omega)$, Kerr rotation θ_{K}, and ellipticity ε_{K} of Ni. Solid curves: equilibrium spectra as given in figure 1; dotted curves: non-equilibrium spectra obtained within model A for $n_{\mathrm{p}} = 0.1$ excited electrons; dashed curves: non-equilibrium spectra obtained within model B for $n_{\mathrm{p}} = 0.01$.

3. Results and discussion

Figure 6 shows a comparison of the equilibrium frequency-dependent conductivity tensor and complex Kerr angle (cf figure 1) with the corresponding non-equilibrium spectra obtained within the two models specified in the previous section.

In model A the zero-temperature MOKE signal is changed for two reasons: near the Fermi level optical transitions are partly blocked because of the reduction of $f_\sigma^<$ from unity and the non-zero values of $f_\sigma^>$. In addition, previously forbidden transitions entirely below and above E_{F} are now allowed due to the small steps in the modified electron distributions. For illustrative purposes we assume $n_{\mathrm{p}} = 0.1$. All elements of the conductivity tensor are found to be reduced as a result of the depletion. Substantial reductions are obtained for the real and imaginary parts of the diagonal element $\sigma_{xx}(\omega)$. Somewhat smaller changes are found for $\sigma_{xy}(\omega)$. The absorptive part $\mathrm{Re}[\sigma_{xx}]$ is depleted over a rather broad energy range (0 up to 2.2 eV) due to the 1.7 eV wide distributions of holes and excited electrons assumed in model A. The dispersive spectrum $\mathrm{Im}[\sigma_{xx}]$ is depleted over an even wider energy range as a result of the Kramers–Kronig relation. In spite of this, the modifications of the Kerr rotation and ellipticity caused by depletion are considerably smaller as a result of partial cancellations. Since the Kerr angle is mainly governed by the ratio $\sigma_{xy}(\omega)/\sigma_{xx}(\omega)$, this quantity naturally changes relatively little as long as the components of σ_{ij} are affected similarly by the depletion.

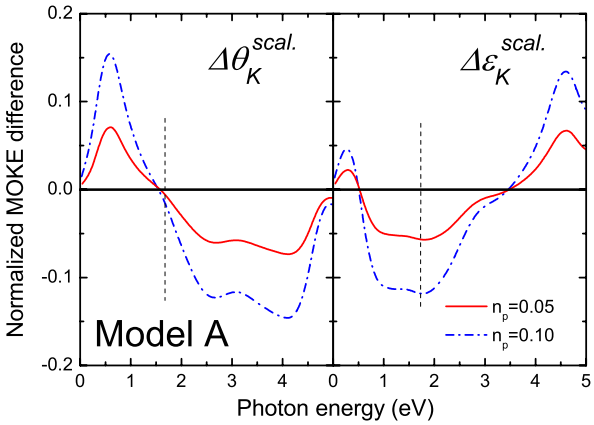

Figure 7. Normalized changes of the Kerr rotation $\Delta\theta_{\rm K}^{\rm scal} = \Delta\theta_{\rm K}/\theta_{\rm K}$ (1.7 eV) and ellipticity $\Delta\varepsilon_{\rm K}^{\rm scal} = \Delta\varepsilon_{\rm K}/\varepsilon_{\rm K}$ (1.7 eV) due to non-equilibrium electron distributions obtained within model A for excited electron numbers $n_{\rm p} = 0.05$ and 0.1.

To illustrate the modifications of the Kerr angle more clearly we show in figure 7 the relative change of the rotation and ellipticity spectra, for $n_{\rm p} = 0.05$ and 0.1. The relative rotation and ellipticity spectra have been normalized to the respective equilibrium value at the pump-laser energy 1.7 eV. Thus, if the probe-laser energy coincides with this energy, we have the quantities $\Delta\theta_{\rm K}/\theta_{\rm K}$ and $\Delta\varepsilon_{\rm K}/\varepsilon_{\rm K}$ studied in [3]. For $n_{\rm p} = 0.1$ the relative change of the Kerr rotation and ellipticity are seen to reach up to about 10%. Correspondingly smaller changes are obtained for $n_{\rm p} = 0.05$. Assuming $n_{\rm p} = 0.012$, as estimated for the experiment [3], model A would predict changes of the order of 1% only, while the experiment gave changes of about 10%.

These results suggest that the step-like non-equilibrium electron distributions used in model A lead to significantly smaller changes in the complex Kerr angle than those detected experimentally for Ni. As already pointed out above, the reason for this failure of the simple non-equilibrium picture is presumably the underlying assumption that the excited electrons and holes are spread uniformly over the entire 1.7 eV wide energy windows below and above $E_{\rm F}$. Thus, the peculiar state blocking characteristic of optical techniques, namely, the pairing of states separated by the laser frequency and by the direct nature of the transition (i.e., its confinement to small regions in k-space), are missing from model A.

To improve upon this model we show in figure 6 also the analogous conductivity and Kerr angle spectra computed for model B. It is evident that the frequency variation of the changes differs markedly from the more or less uniform reduction found in model A. The key effect of the reduced occupation differences $f_{n\sigma}^{<} - f_{m\sigma}^{>}$ is the reduction of the absorptive parts of the conductivity, i.e., of $\mathrm{Re}[\sigma_{xx}(\omega)]$ and of $\mathrm{Im}[\sigma_{xy}(\omega)]$, at frequencies close to the pump-laser frequency. By construction, we assumed $f_{n\sigma}^{<} - f_{m\sigma}^{>}$ to deviate from unity only within a window of width $D = 0.2$ eV about 1.7 eV. Away from this frequency, the probe laser detects essentially the standard equilibrium condition. As a result of the Kramers–Kronig relations, the dispersive components $\mathrm{Im}[\sigma_{xx}(\omega)]$ and $\mathrm{Re}[\sigma_{xy}(\omega)]$ are changed in a wider energy range than the absorptive components. These dispersive components exhibit in addition a sinusoidal frequency dependence, with a vanishing change close to 1.7 eV. Small shifts and asymmetries arise from the frequency dependence of the absorptive parts near 1.7 eV.

It is now evident from these modifications of the real and imaginary components of the conductivity tensor that the complex Kerr angle can be subject to a more complex frequency

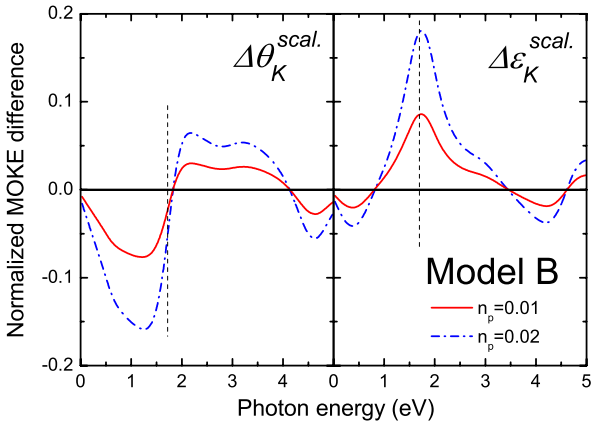

Figure 8. As figure 7, but for non-equilibrium electron distributions obtained within model B for $n_p = 0.01$ and 0.02.

variation as well. This is illustrated in figure 8 where we show the relative change of the rotation and ellipticity spectra, normalized with respect to the equilibrium values at the pump-laser energy 1.7 eV, for $n_p = 0.01$ and 0.02. For the experimentally determined excitation density $n_p = 0.01$ we now find changes in the rotation and ellipticity of the order of 5–10%, i.e., comparable to the experimental results [3]. A second important conclusion can be drawn from figure 8. The relative Kerr rotation and ellipticity changes are clearly disproportional under the non-equilibrium condition, as has been observed in a number of pump–probe experiments [3, 14–17]. In figure 8 the state blocking causes a smaller Kerr rotation at 1.7 eV, which is evidently not related to a magnetization drop. Conversely, the optical bleaching causes ε_K to become larger. A disproportionality between the relative changes in the rotation and ellipticity are also obtained for model A (see figure 7). At about 1.7 eV both the rotation and ellipticity are reduced by the non-equilibrium conditions, yet the ellipticity is reduced six times more. Thus, both kinds of non-equilibrium distributions generate changes in the Kerr rotation and ellipticity that are purely of optical origin and unrelated to any magnetization changes.

4. Conclusion

We have investigated the magneto-optical Kerr effect during the initial stages of the electron thermalization process right after the high-intensity pump laser has generated a non-equilibrium electron distribution. Two different models for the bleaching or state-blocking mechanism are considered which lead to modifications of the optical conductivity tensor compared to standard equilibrium conditions. In model A the electrons and holes excited by the pump laser are distributed evenly within the energy windows $E_F \pm \hbar\omega_p$. Thus, the occupation numbers are step-like functions of energy, where the step sizes depend only on band and spin indices. As a result, certain optical transitions close to E_F are blocked, whereas new transitions between band pairs completely below or above E_F are allowed. For the experimental excitation density of about 0.01 electrons per atom, the changes of the Kerr rotation and ellipticity are of the order of 1%, i.e., much smaller than observed in the MOKE experiment. To capture better the underlying physics we considered an alternative model B which accounts for the fact that in an optical measurement pairs of spin bands separated by $\hbar\omega_p$ are particularly sensitive to state blocking. Consequently, the excited holes and electrons are now confined to rather narrow energy windows about the pump-laser frequency and thereby to the small k-space regions in which optical transitions take place. This picture leads to much larger changes in the conductivity components than model A. For the experimental excitation density the

Kerr rotation and ellipticity are modified by about 5%–10%, in qualitative agreement with the experimental data. Since the sample magnetization is not changed by the pump laser, these modifications imply that the Kerr signal during the thermalization of the electron gas is not proportional to the magnetization. Moreover, a disproportionality between the Kerr rotation and ellipticity responses is found for both non-equilibrium distributions of model A and B. This result demonstrates that modifications of the Kerr quantities are not related to a magnetization change but caused by state-blocking effects. Thus, the Kerr response at ultrashort times after the pump-laser pulse cannot be taken as a measure of the demagnetization process.

Acknowledgments

We gratefully acknowledge valuable comments from B Koopmans, M Münzenberg, and T Kampfrath. AL acknowledges support by the European Network 'Dynamics' (Project No (SFM) DE000194).

References

[1] Beaurepaire E, Merle J-C, Daunois A and Bigot J-Y 1996 *Phys. Rev. Lett.* **76** 4250
[2] Ju G, Vertikov A, Nurmikko A V, Canady C, Xiao G, Farrow R F C and Cebollada A 1998 *Phys. Rev.* B **57** R700
[3] Koopmans B, van Kampen M, Kohlhepp J T and de Jonge W J M 2000 *Phys. Rev. Lett.* **85** 844
[4] Scholl A, Baumgarten L, Jacquemin R and Eberhardt W 1997 *Phys. Rev. Lett.* **79** 5146
[5] Aeschlimann M, Bauer M, Pawlik S, Weber W, Burgermeister R, Oberli D and Siegmann H C 1997 *Phys. Rev. Lett.* **79** 5158
[6] Hohlfeld J, Matthias E, Knorren R and Bennemann K H 1997 *Phys. Rev. Lett.* **78** 4861
[7] Güdde J, Conrad U, Jähnke V, Hohlfeld J and Matthias E 1999 *Phys. Rev.* B **59** R6608
[8] Crawford T M, Silva T J, Teplin C W and Rogers C T 1999 *Appl. Phys. Lett.* **74** 3386
[9] Regensburger H, Vollmer R and Kirschner J 2000 *Phys. Rev.* B **61** 14716
[10] Hohlfeld J, Wellersdorf S-S, Güdde J, Conrad U, Jähnke V and Matthias E 2001 *Chem. Phys.* **251** 237
[11] Beaurepaire E, Maret M, Halté V, Merle J-C, Daunois A and Bigot J-Y 1998 *Phys. Rev.* B **58** 12134
[12] Hübner W and Zhang G P 1998 *Phys. Rev.* B **58** R5920
[13] Zhang G P and Hübner W 2000 *Phys. Rev. Lett.* **85** 3025
[14] Kampfrath T, Ulbrich R G, Leuenberger F, Münzenberg M, Sass B and Felsch W 2002 *Phys. Rev.* B **65** 104429
[15] Koopmans B, van Kampen M, Kohlhepp J T and de Jonge W J M 2000 *J. Appl. Phys.* **87** 5070
[16] Guidoni L, Beaurepaire E and Bigot J-Y 2002 *Phys. Rev. Lett.* **89** 017401
[17] Kampfrath T 2001 *Masters Thesis* University of Göttingen
[18] Wilks R, Hughes N D and Hicken R J 2002 *J. Appl. Phys.* **91** 8670
[19] Del Fatti N, Voisin C, Achermann M, Tzortzakis S, Christofilos D and Vallée F 2000 *Phys. Rev.* B **61** 16956
[20] Voisin C, Christofilos D, Del Fatti N, Vallée F, Prével B, Cottancin E, Lermé J, Pellarin M and Broyer M 2000 *Phys. Rev. Lett.* **85** 2200
[21] Oppeneer P M, Maurer T, Sticht J and Kübler J 1992 *Phys. Rev.* B **45** 10924
[22] Kraft T, Oppeneer P M, Antonov V N and Eschrig H 1995 *Phys. Rev.* B **52** 3561
[23] Williams A R, Kübler J and Gelatt C D 1979 *Phys. Rev.* B **19** 6094
[24] Oppeneer P M 2001 Magneto-optical Kerr spectra *Handbook of Magnetic Materials* vol 13, ed K H J Buschow (Amsterdam: Elsevier) pp 229–422
[25] van Engen P G 1983 *PhD Thesis* Technical University Delft
[26] Di G Q and Uchiyama S 1994 *J. Appl. Phys.* **75** 4270
Di G Q 1995 private communication
[27] Liebsch A 1979 *Phys. Rev. Lett.* **43** 1431
[28] Argyres P N 1954 *Phys. Rev.* **97** 334
[29] Oppeneer P M, Sticht J, Maurer T and Kübler J 1992 *Z. Phys.* B **88** 309
[30] Koopmans B, van Kampen M and de Jonge W J M 2003 *J. Phys.: Condens. Matter* **15** S723